Journal of Asian Earth Sciences xxx (xxxx) xxx–xxx

Contents lists available at ScienceDirect

Journal of Asian Earth Sciences

journal homepage: www.elsevier.com/locate/jseaes

Full length article

Large Himalayan Frontal Thrust paleoearthquake at Khayarmara in eastern Nepal

Steven G. Wesnousky[a,*], Yasuhiro Kumahara[b], Deepak Chamlagain[a,c], Prajwal Chandra Neupane[c]

[a] Center for Neotectonic Studies and Seismological Laboratory, University of Nevada, Reno, Reno, NV 89557, USA
[b] Graduate School of Education, Hiroshima University, 1-1-1, Kagamiyama, Higashi-Hiroshima City, Hiroshima 739-8524, Japan
[c] Department of Geology, Tri-Chandra M. Campus, Tribhuvan University, Nepal

ARTICLE INFO

Keywords:
Himalaya
Paleoseismology
Tectonics
Seismic hazard
Nepal

ABSTRACT

An exposure created by excavation of a trench across the Himalayan Frontal Thrust provides the basis to interpret that a single earthquake produced vertical separation of ~7 m at Khayarmara, a small community ~80 km southwest of Kathmandu. The fault trace at Khayarmara is expresssed by a topographic ridge resulting from folding up-dip and toward the surface at the expense of greater fault slip taking place at depth. Structure, stratigraphy, and radiocarbon data are interpreted to indicate displacement occurred after about 1050 CE to 1200 CE. The timing and displacement at Khayarmara are compared to that reported previously at six contiguous sites that extend from 200 km to the west and 250 km to the east of Khayarmara, respectively. The comparison leads us to conclude that the surface rupture at Khayarmara was part of a ≥250 km long synchronous surface rupture earthquake of magnitude approaching if not surpassing Mw 9. We observe in the exposure no record of surface rupture associated with the great 1934 Bihar-Nepal earthquake.

1. Introduction

The Himalayan Frontal Thrust (HFT) of eastern Nepal dips northward from its trace to merge with the Main Himalayan Thrust (MHT) that extends ~120 km northward to beneath the High Himalaya (Fig. 1; Seeber and Armbruster, 1981). The MHT exhibits no evidence of aseismic slip and is generally considered to slip only during recurrent large earthquakes that function to accommodate ~20 mm/yr of convergence between India and Tibet (Bilham et al., 1997). The 2015 Mw 7.8 Gorkha earthquake was confined to a down dip section of the MHT and serves as the most recent illustration of this process (Avouac et al., 2015). Earthquakes much larger than the Gorkha event may be expected if the entire down-dip width of the MHT slips to produce surface rupture along the HFT. A number of geologic studies along the HFT of eastern Nepal assessing the age, size, and recurrence time of prehistoric earthquakes now provide support for the expectation (Fig. 1 and Lave et al., 2005; Upreti et al., 2000; Wesnousky et al., 2017a, 2017b). We here add to these studies our findings arising from study of a trench excavated across the HFT adjacent to Khayarmara Khola in eastern Nepal. The paper concludes with a discussion of our interpretations at Khayarmara in the context of the previous studies along the HFT and the potential for great earthquakes along the section of the HFT southward of the recent Gorkha earthquake.

2. Khayarmara site

The Khayarmara site is located ~7 km west and ~50 km east of earlier paleoseismic studies along the HFT at Marha Khola (Lave et al., 2005) and Bagmati (Wesnousky et al., 2017a), respectively, and south of the 2015 Gorkha earthquake aftershock zone (Fig. 1). A photo and surficial geologic map showing the exact location of the site are in Fig. 2. The southern of two traces of the HFT strikes eastward across the flood plain deposits (unit Qfb) of the Khayarmara Khola. Displacement along the southern trace has led to uplift and abandonment of older flood plain deposits (unit Qfa). Additional and older offsets are recorded along the northern trace by the uplift of a yet older strath of fluvial deposits (Qto) and Siwalik bedrock. A topographic profile across the transect shown in Fig. 2 is presented in Fig. 3 and illustrates the location and extent of the trench excavation in relation to the scarp profile. The abrupt surface expression of the scarp approaches 5 m in height. The crest of the south-facing scarp exhibits a distinct topographic bulge from which the elevation decreases northward into a smooth hanging wall surface that is inclined slightly northward. The bulge above the scarp and the inclination of the hanging wall northward are here interpreted to suggest that the fault beneath the profile is characterized by a degree of convex-upward curvature and that the total slip along the fault is increasingly accommodated up-dip toward

* Corresponding author.
E-mail address: wesnousky@unr.edu (S.G. Wesnousky).

https://doi.org/10.1016/j.jseaes.2019.01.008
Received 7 September 2018; Received in revised form 3 January 2019; Accepted 3 January 2019
1367-9120/

Please cite this article as: Steven G. Wesnousky, et al., Journal of Asian Earth Sciences, https://doi.org/10.1016/j.jseaes.2019.01.008

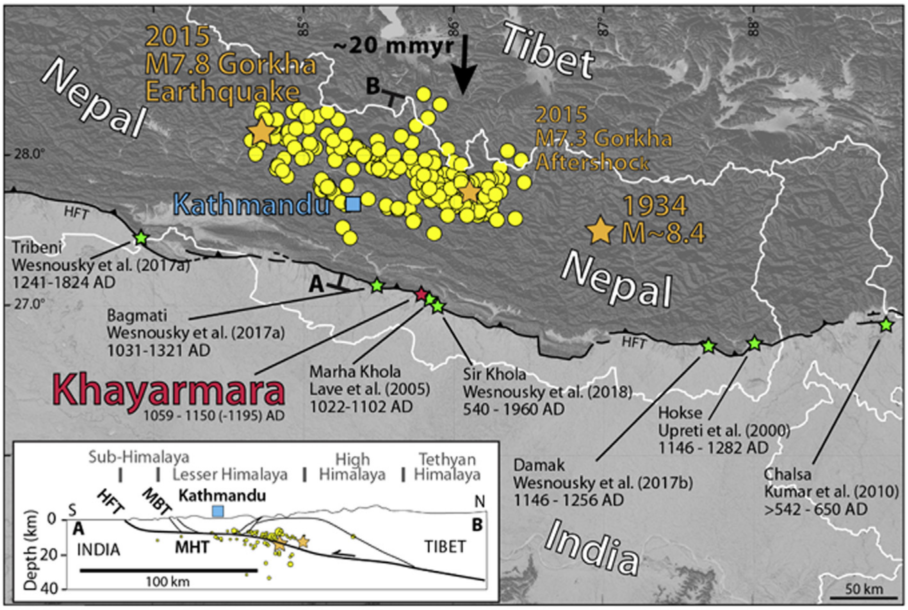

Fig. 1. Location of Khayarmara (red star) in relationship to other paleoearthquake study sites (green stars) along the HFT of eastern Nepal. Sites are labeled to show age of the last large surface displacement and authors reporting the results. Aftershock (yellow dots), mainshock and largest aftershock locations (orange stars) of the 2015 Gorkha earthquake are from NSC (2015). Relationship of the HFT to the Main Himalayan Frontal Thrust (MHT) is shown in the inset. Interpretations of geodesy indicate that displacement on the MHT accommodates on average ~20 mm/yr of north-south shortening (e.g., Stevens and Avouac, 2015). See text for further discussion. (For interpretation of the references to color in this figure legend, the reader is referred to the web version of this article.)

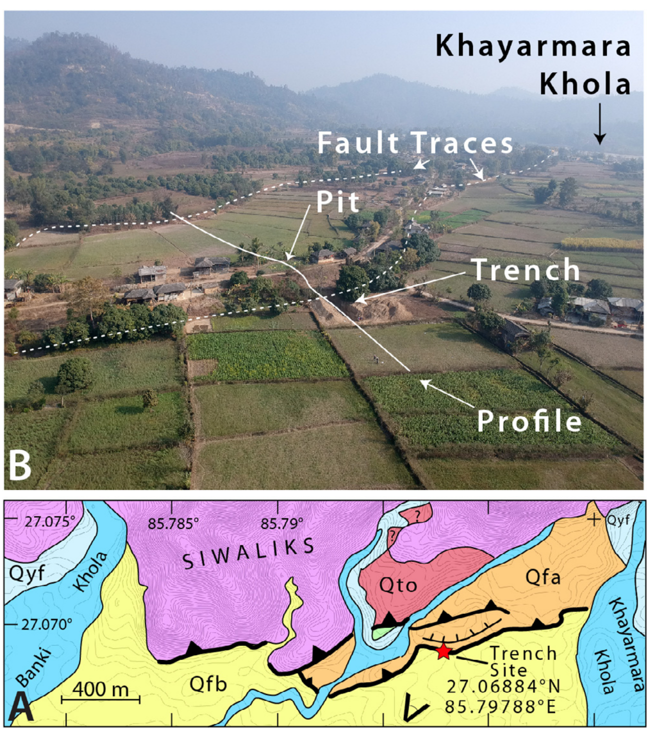

Fig. 2. (upper) Annotated oblique photo and (lower) surficial geologic map of Khayarmara trench site. See text for unit descriptions. Qyf are youngest flood plain deposits. Orientation and breadth of photo shown approximately by open end of angle symbol on map. Trace of HFT on map depicted by solid black lines with triangles on hanging wall. The subparallel scarp to the north of trench was not studied in detail and our observations insufficient to conclude whether or not the subparallel scarps formed simultaneously. Contour interval is 2 m constructed from SRTM 1 Arc-Second Global data downloaded from http://earthexplorer.usgs.gov).

the surface by folding at the expense of fault slip taking place at depth (Fig. 3).

3. Stratigraphy, structure, and paleoearthquake displacement

A sketch of the west wall of the trench exposure is shown in Fig. 4 and photos of the exposure in Fig. S1 of the Supplementary Information. The exposure is about 20 m long reaching a maximum depth of about 5.5 m. Unit 1 comprises much of the north half of the exposure. It is primarily poorly-sorted rounded pebble and cobble gravel with occasional small boulders. Gravel layers and lenses are distinguished by distinct variations in clast size and define a south dipping fabric that generally parallels the upper contact of the unit. The lower southern contact of the unit is abrupt, dips ~16° to the north, and is interpreted to be a fault contact that has emplaced Unit 1 over Unit 2, a generally massive brown very fine sandy silt deposit locally displaying a few percent coarse sand and small pebbles near the fault contact. Unit 2′ deposits are similar in texture and color to those of Unit 2 and located on the sloping upper contact of Unit 1. The location of Unit 3 deposits on the slope of the upper contact of Unit 1 has led to erosion and thinning of Unit 2′. A pit excavated on the surface above the exposure (Fig. 3) shows a complete ~1.3 m section of the Unit 2′ deposits resting on gravel of Unit 1 (Fig. 5). Resting on and in angular contact with Units 1, 2 and 2′ are generally horizontal deposits of Unit 3. Unit 3a is very fine sandy silt with concentrations of well-sorted fine sand that exhibit cross-laminae that impart a horizontal fabric to the unit. Unit 3b is generally poorly-sorted rounded pebble and cobble gravel in which discontinuous beds and lenses of coarse sand also define a horizontal fabric. The Unit 3b interfingers with Unit 3a at its base. Unit 3c is in contrast primarily very fine sandy silt locally containing within and at its base very dark black organic clay rich horizons. Unit 3d is a pocket of gravel similar in texture to unit 3b.

A sketch and photos of the east trench wall (Figs. 6 and S2) exhibits the same general structure and stratigraphy though is more limited in extent because portions of the trench wall collapsed. The exposure adds several observations important to interpretation. Unit 2 resides in depositional contact on fluvial gravels of the same texture as Unit 1 and together exhibit the same stratigraphy as observed in the pit shown in Fig. 5. Additionally, Unit 2 is again observed to be faulted but in this exposure Unit 2 is observed to continuously wrap around the southern extent of Unit 1 to where it is also present on the south-dipping Unit 1 gravel. The observations give reason to interpret that the Unit 2′ deposits of the west wall exposure (Fig. 3) and the capping fine grained deposits observed in the pit (Figs. 3 and 5) are faulted continuations of Unit 2. The basal fault and overlying splay fault are essentially flat lying in this east wall exposure.

The stratigraphy and structure are very similar to exposures of the HFT elsewhere along strike and similarly interpreted: The fine grained

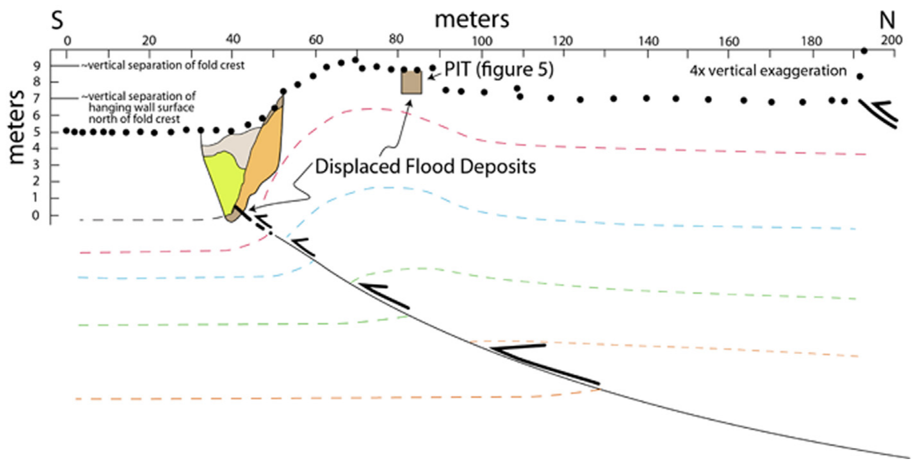

Fig. 3. Elevation profile (black dots) and length and depth extent of trench (colored area). Dashed lines (e.g. layer boundaries) and arrows (slip on fault) schematically illustrate the idea that the total slip along the fault is increasingly accommodated up dip and near the surface by folding at the expense of greater fault slip taking place at depth. Location of trench and profile marked in Fig. 2. Photo of pit provided in Fig. 5. Flood deposits on foot and hanging wall are interpreted to have been contiguous prior to displacement. Vertical accuracy of the points on the profile is < ~2 cm. Vertical separation measured from surface of flood deposits on footwall. No evidence of faulting is suggested in the geomorphology between the trench and pit exposure.

deposits of Unit 1 and Unit 2 are interpreted to originally be flat lying and representative of a broad floodplain whereby fluvial gravel of the Khayarmara Khola system (Unit 1) is overlain by finer grained flood (overbank) deposits (Unit 2). Subsequent displacement on the fault exposed in the trenches has resulted in folding of units 1 and 2 on the hanging wall to produce a dip panel, and southward translation of the hanging wall to produce a duplication or repetition of Units 1 and 2 stratigraphy above fault plane.

Estimation of the exact amount of fault slip needed to produce the Khayarmara scarp is problematic because the exposure of the fault plane is limited and no direct measure of the fault dip is available across the entire extent of the scarp. Assuming Unit 2 was the ground surface at the time slip initiated, the vertical separation across the scarp is 9–10 m when measured to the scarp crest or ~7 m when measured with respect to the unfolded surface north of the crest (Fig. 3). The 9–10 m measure may reflect in part local shortening at the tip of the scarp, similar to that which occurs upon horizontally pushing the edge of a carpet. The 7 m measure is probably more representative of the vertical displacement due to translation along the fault. The dip of the fault in the trench exposures is from 0 to 16°. Assuming a fault dip of ~30° beneath the back tilted surface, as may be expected from simple frictional considerations (e.g., Anderson, 1951) though significantly greater than observed in the trench, the displacement required to produce the uplift would need to be twice the observed vertical displacement, about ~14 m. The assumption of fault dips observed in the trench exposures would require yet more displacement to explain the observed vertical separation.

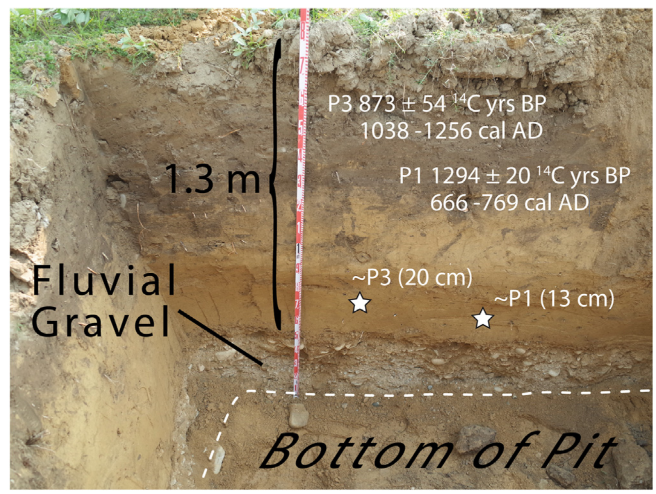

Fig. 5. Pit exposure reveals light brown very fine sandy silt deposits capped by dark brown organic rich active soil horizon resting on coarse sand, pebble, and small cobble river gravel. Location of pit is on surface of fault and fold scarp is shown in Figs. 2 and 3. Detrital charcoal samples P1 and P3 were sampled at 13 and 20 cm above the underlying fluvial gravel layer, respectively.

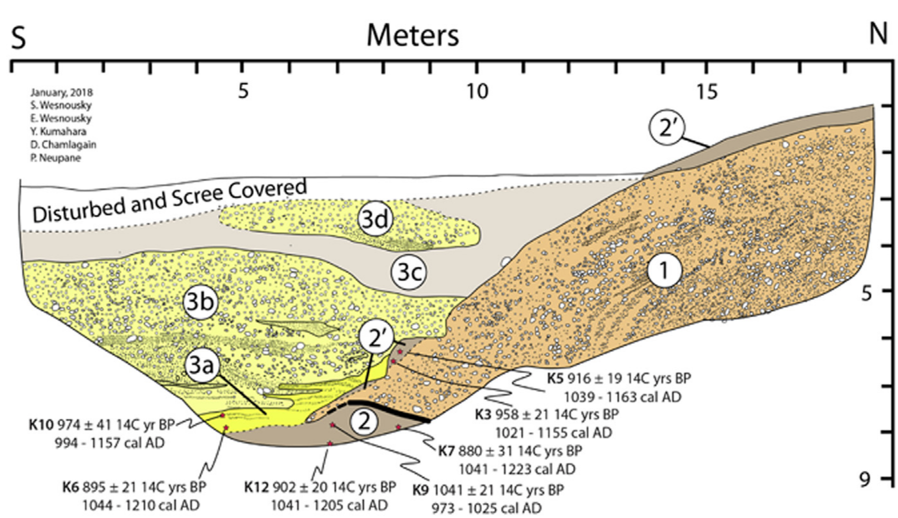

Fig. 4. Sketch of west wall of trench exposure. Units are numbered sequentially from oldest to youngest. The fault is shown by thick black line, and locations and ages of detrital charcoal samples are shown by small red stars and associated labels, respectively. (For interpretation of the references to color in this figure legend, the reader is referred to the web version of this article.)

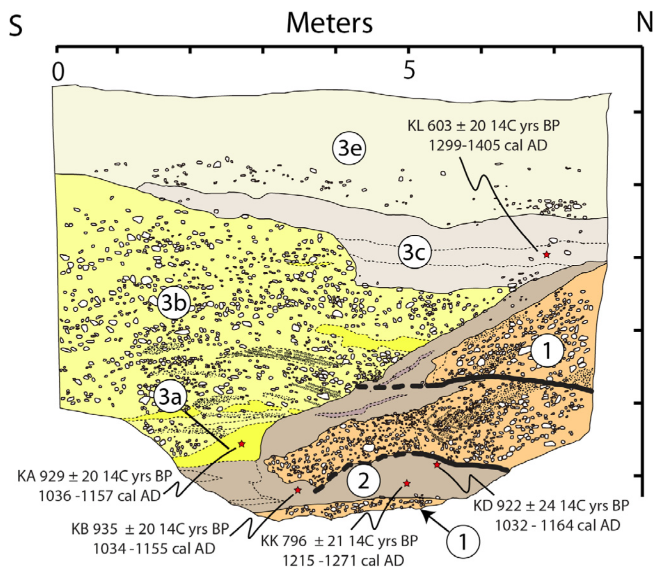

Fig. 6. Sketch of east wall of trench exposure. Units numbers are labeled sequentially from oldest to youngest and match those in Fig. 4. Fault strands are shown by thick black lines, and locations and ages of detrital charcoal samples are shown by small red stars and associated labels, respectively. (For interpretation of the references to color in this figure legend, the reader is referred to the web version of this article.)

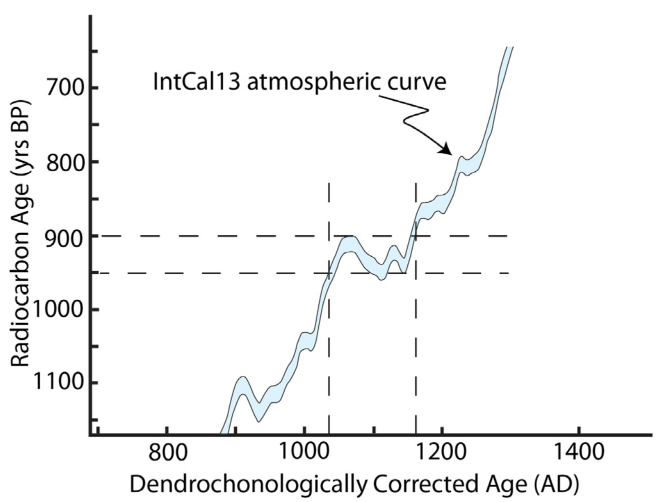

Fig. 7. Portions of IntCal13 atmospheric (dendrochronological) correction curve of Reimer et al. (2013). Radiocarbon ages of detrital charcoal samples bounding the displacement horizon at Khayarmara are largely within the range of 900–950 14C yrs. The range and attendant uncertainty of dendrochronologically corrected ages is greater for samples with 14C yrs between 900 and 950 14C yrs because the IntCal13 atmospheric curve is relatively level and exhibits slope reversals.

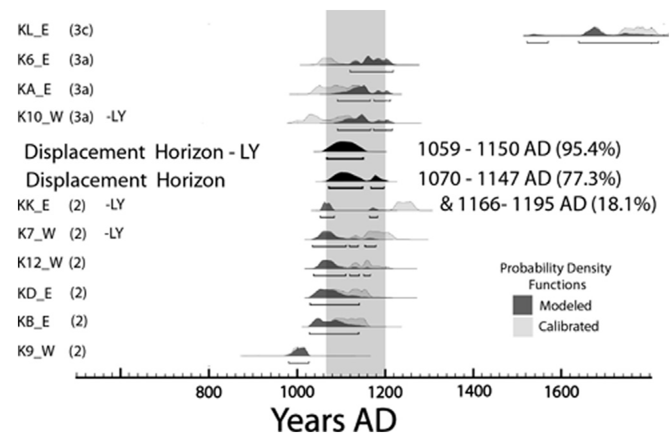

Fig. 8. Radiocarbon age probability density distributions of detrital charcoal samples are arranged in general stratigraphic order above and below the displacement horizon. Sample numbers and the horizon from which they were sampled are shown at the left of the plot. Calibrated and modeled aand the age of the displacement horizon are calculated with Oxcal (https://c14.arch.ox.ac.uk/oxcal/OxCal) and the IntCal13 atmospheric curve of Reimer et al. (2013). Samples marked LY exhibited low yield of organic carbon in processing. Calculations of the displacement horizon are shown for both the entire data set and with low-yield (-LY) samples removed. The shaded bar delimits the age range for the displacement horizon. Modeled ages for respective samples correspond to OxCal model including entire data set.

4. Radiocarbon observations

The location of detrital charcoal samples collected from the trench exposures are displayed in Figs. 4 and 6. Labels in the figures show the radiocarbon (14C yrs BP) and dendrochronologically corrected (cal AD) ages calculated for each sample. The locations include samples located in deposits emplaced prior (unit 2) and subsequent to (units 3) the fault displacement and deformation that produced the Khayarmara scarp and dip panel, and thus the means to place temporal bounds on the displacement. The ages of samples from units 2 and 3 are closely grouped, show overlap (lack of stratigraphic order between and within units) and generally fall within a close range of 900–950 14C yrs BP. The two observations limit the resolution to which the temporal bounds on the displacement may be placed. The period from 900 to 950 C14 yrs BP marks a relatively flat portion of the dendrochronological correction curve that exhibits multiple changes in slope (Fig. 7). A 14C age within this range may correlate to multiple corrected (cal AD) ages between a relatively broader range of 1040–1160 CE. An analytical report for each radiocarbon sample is provided in the Table S1 of accompanying Supplementary Information.

The corrected ages of samples from Units 2 and 3 are shown in light gray in Fig. 8 such that they are grouped below and above the displacement horizon: the boundary between faulted and unfaulted deposits in the exposure. The ages within each group are arranged in the figure such that they are younger in age upward but not necessarily in strict stratigraphic order within the respective units. Application of Oxcal (Bronk, 2009; https://c14.arch.ox.ac.uk/oxcal/OxCal) provides the means to estimate a set of model ages for each sample and the timing of the displacement horizon that is most likely, given the stratigraphic order of the samples. The program is applied here with the assumptions that samples from units 2 and 3 comprise 'phases' whereby it is recognized that there is no firm information on the stratigraphic order of samples within each unit, and that the detrital charcoal samples were deposited near in time to carbon fixation. The modeled ages are depicted in dark gray in Fig. 8 and the age of the displacement horizon is computed between 1070 and 1195 CE. Corrected and modeled ages of a number of samples do not overlap significantly. Charcoal is generally 45–85% carbon by mass. A number of the samples have significantly less carbon yields (Table S1). Removal of these samples (marked –LY) and reapplication of Oxcal leads to a model whereby modeled ages generally agree with corrected ages and smaller time window for the event horizon estimated at 1059–1150 CE (Figs. 8 and S3). The low carbon yields might simply be due to retention of inorganic clays or sands making it through the purification protocol (Greg Hodgins, University of Arizona, Personal Communication). Inorganics as such do not necessarily affect the reliability of the 14C ages, though are here observed to have ages that fall on the edges of the distribution of ages observed above and below the event horizon. In any case, the removed samples exceed anticipated uncertainties and the calculation illustrates that the total breadth of uncertainty attached to the calculation of a displacement horizon is not necessarily encompassed by the formal uncertainties provided by a single OxCal model. The uncertainty is yet further broadened when considering that the detrital charcoal samples represent a maximum age of the deposit from which they are sampled (e.g., Blong and Gillespie, 1978; Frueh and Lancaster, 2014; Gavin, 2001), in which case it may be reasoned that the earthquake displacement occurred subsequent to the event horizon defined by Oxcal and the youngest charcoal age 1215–1271 CE recorded for the low yield sample KK found in deposits unbroken by the fault.

5. Discussion and conclusion

The folding that accompanies recent fault displacements in young sediments along the HFT is generally expressed by the presence of a dip panel similar to that preserved in the dipping Unit 1 at Khayarmara (Figs. 4 and 6; e.g., Kumar et al., 2001; 2006; 2010; Lave et al., 2005; Wesnousky et al., 2017a, 2017b). The folding is particularly well expressed at Khayarmara where the degree of shortening and folding is of such a large amount that the trace of the HFT is marked by a long linear ridge (Figs. 2 and 3).

The 2015 Gorkha M7.8 earthquake rupture did not extend sufficiently southward to produce surface rupture along the HFT (Fig. 1; e.g., Angster et al., 2015; Avouac et al., 2015; Hayes et al., 2015). It has been inferred that the nearby larger M ∼8.4 Bihar-Nepal earthquake of 1934 was the result of displacement on the MHT (Molnar and Deng, 1984). The presence of surface rupture on the HFT that may be attributed to the 1934 earthquake is not observed in the Khayarmara trench. Clear evidence for surface rupture on the HFT that may be attributed to the 1934 event is likewise not observed to be present at nearby sites of similar study at Sir Khola, Marha Khola, Bagmati and elsewhere along the HFT (Fig. 1 and Lave et al., 2005; Wesnousky et al., 2017a, 2017b; 2018).

The stratigraphy, structure, and radiocarbon data point to displacement and formation of the Khayarmara scarp at some time after about 1060 and 1195 CE (Fig. 8). Unit 2 is horizontal where exposed south of the dipping panel of Unit 1 (Figs. 4 and 6). Unit 3 is in conformable depositional contact with Unit 2 and most simply interpreted as stratigraphy that has accumulated on and against the scarp after fault slip and formation of the Unit 1 dip panel. The horizontal fabric and beds of Unit 3 are devoid of any angular unconformities that might be attributed to tectonic deformation during its deposition and provide justification to interpret that the deformation and scarp at Khayarmara were formed during a single earthquake displacement producing ∼7 m of vertical separation. If slip along the subparallel scarp to the north (Fig. 1) occurred contemporaneously, the total coseismic displacement could be significantly greater.

Figs. 1 and 9 provide a basis to compare the timing of the Khayarmara displacement to the timing of the most recent surface ruptures previously identified elsewhere along the HFT of eastern Nepal. The radiocarbon ages reported for samples collected at each site are compiled in Fig. 9: the calibrated and modeled ages of each sample and displacement horizon calculated with Oxcal are shown for each site. The calculated displacement horizons in each case again assume that the detrital charcoal samples were deposited near in time to carbon fixation. The formal uncertainties accompanying the displacement horizon estimates overlap around 1100 CE at Bagmati, Khayarmara, Marha Khola, Sir Khola and Damak, a distance of ∼250 km along the HFT. A thrust earthquake averaging ∼7 m of coseismic slip is on average expected to be associated with a rupture length approaching 400 km and a moment magnitude of 8.3 (Leonard, 2014). The vertical separation at the Khayarmara scarp is ∼7 m and may be viewed as a minimum of the amount of coseismic fault slip required to produce the scarp, and thus the rupture length and moment magnitude of the earthquake that produced the scarp at Khayarmara may well have exceeded these values. Values of vertical separation across the scarps produced by the most recent displacements at Bagmati (∼7 m), Marha

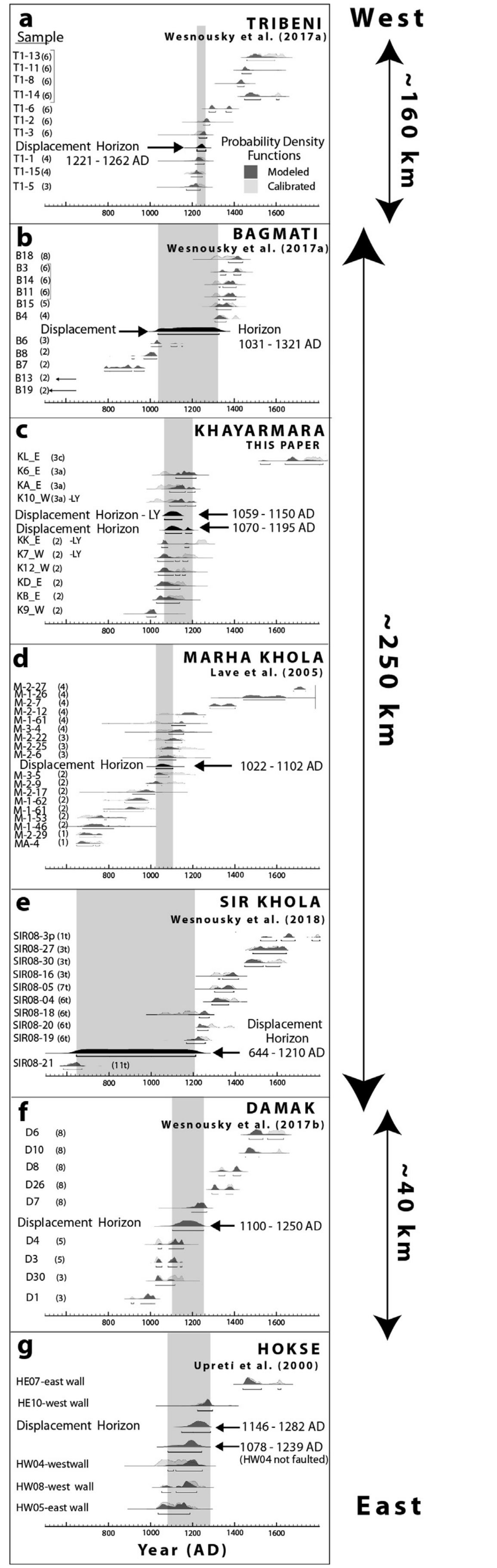

(caption on next page)

Fig. 9. Compilation of radiocarbon observations at each of the paleoearthquake study sites along the HFT shown in Fig. 1. See Fig. 8 caption for explanation. Shaded bars provided to aid comparison of timing of displacement horizons between sites.

Khola (∼7 m), and Damak (∼5.5 m) are of similar size (Lave et al., 2005; Wesnousky et al., 2017a, 2017b). In this context, it follows that this ∼250 km section of the HFT ruptured simultaneously sometime around ∼1100 CE. The displacement horizon at Hokse does not overlap in time with all of the preceding sites and might be cited to suggest that an ∼1100 CE rupture did not continue another 40 km eastward of Damak. The displacement horizon at Hokse though is based on a very limited number of radiocarbon ages and is critically dependent on a single sample (HW04) that is ambiguously presented as faulted in the original publications of Upreti et al. (2000, 2007) (Fig. S4). It is thus difficult to confidently rule out that Hokse did not rupture simultaneously in ∼1100 CE with the sites to the west, or that rupture did not continue yet farther to the east of Hokse. In contrast, the radiocarbon observations reported by Wesnousky et al. (2017a) at Tribeni, ∼160 km west of Bagmati, seem to preclude the occurrence of displacement prior to ∼1200 CE. If we return to the idea that the calculated event horizons are minimum estimates because they are based on detrital charcoal, one may also conjecture that all of the sites ruptured simultaneously sometime after ∼1200 CE. This thinking has previously been used to assert displacements at a subset of the sites along the HFT in Fig. 9 correlate to the limited account by Pant (2002) of an historical earthquake that produced damage in Kathmandu in 1255 CE (e.g., Bollinger et al., 2016), though historical records appear insufficient to rule out the possibility of an earlier time of rupture.

The radiocarbon data by themselves certainly do not prove the occurrence of simultaneous rupture at sites extending ∼250 km from Bagmati to Damak, or the greater length of ∼450 km between Tribeni and Hokse. Our assertion that at least ∼250 km of the arc ruptured simultaneously is influenced, in addition to the large displacements recorded in the trenches, by the tectonic setting and independent geodetic analyses. The continuous ∼2500 km long arc that defines the Himalayan thrust front is of the same form as observed along the globe's major oceanic thrust boundaries (e.g., Molnar et al., 1977; Seeber and Armbruster, 1981), most if not all of which have produced magnitude 8 or 9 thrust earthquakes. Likewise, theoretical arguments have been put forth to conclude that the ongoing pattern of geodetic strain accumulation along the MHT of Nepal requires the recurrence of magnitude Mw 9.0 events every thousand years or so (e.g., Stevens and Avouac, 2016). The geologic data reported here are in concert with these ideas and observations. Finally, multiplying the geodetically observed elastic strain accumulation of ∼20 mm/yr along the Main Himalayan Thrust times the ∼ > 700 years since the last displacement at these sites indicates that sufficient slip (> ∼14 m) is now accumulated to reproduce a similarly great earthquake.

Conflict of interest

The authors declare that there is no conflict of interest.

Acknowledgements

We thank Greg Hodgins for clarifying aspects of radiocarbon analysis and the University of Arizona AMS lab for providing very high precision radiocarbon dates and Roger Bilham and an anonymous reviewer for useful comments. The data used in this publication are embodied in the text and figures and listed in the references. The research was supported by NSF Grant EAR-1345036 and JSPS KAKENHI Grant No. 18KK0027. Center for Neotectonics Studies Contribution No. 76.

Appendix A. Supplementary material

Supplementary data to this article can be found online at https://doi.org/10.1016/j.jseaes.2019.01.008.

References

Anderson, E.M., 1951. The Dynamics of Faulting. Oliver and Boyd, Edinburgh.
Angster, S., Fielding, E.J., Wesnousky, S., Pierce, I., Chamlagain, D., Gautam, D., Upreti, B.N., Kumahara, Y., Nakata, T., 2015. Field reconnaissance after the 25 April 2015 M 7.8 Gorkha earthquake. Seismol. Res. Lett. 86, 1506–1513.
Avouac, J.-P., Meng, L., Wei, S., Wang, T., Ampuero, J.-P., 2015. Lower edge of locked Main Himalayan Thrust unzipped by the 2015 Gorkha earthquake. Nat. Geosci. 8, 708–711.
Bilham, R., Larson, K.M., Freymueller, J., members, P.L., 1997. GPS measurements of present day convergence across the Nepal himalaya. Nature 386, 61–64.
Blong, R., Gillespie, R., 1978. Fluvially transported charcoal gives erroneous 14C ages for recent deposits. Nature 271, 739–741.
Bollinger, L., Tapponnier, P., Sapkota, S.N., Klinger, Y., 2016. Slip deficit in central Nepal: omen for a repeat of the 1344 AD earthquake? Earth Planets Space 68, 12 pp.
Bronk, R., 2009. Bayesian analysis of radicarbon dates. Radiocarbon 51, 337–360.
Frueh, W.T., Lancaster, S.T., 2014. Correction of deposit ages for inherited ages of charcoal: implications for sediment dynamics inferred from random sampling of deposits on headwater valley floors. Quat. Sci. Rev. 88.
Gavin, D.G., 2001. Estimation of inbuilt age in radiocarbon ages of soil charcoal for fire history studies. Radiocarbon 43, 27–44.
Hayes, G.P., Briggs, R.W., Barnhart, W.D., Yeck, W.L., McNamara, D.E., Wald, D.J., Nealy, J.L., Benz, H.M., Gold, R.D., Jaiswal, K.S., Marano, K., Earle, P.S., Hearne, M.G., Smoczyk, G.M., Wald, L.A., Samsonov, S.V., 2015. Rapid characterization of the 2015 M-w 7.8 Gorkha, Nepal, Earthquake sequence and its seismotectonic context. Seismol. Res. Lett. 86, 1557–1567.
Kumar, S., Wesnousky, S.G., Rockwell, T.K., Ragona, D., Thakur, V.C., Seitz, G.G., 2001. Earthquake recurrence and rupture dynamics of himalayan frontal thrust, India. Science 294, 2328–2331.
Kumar, S., Wesnousky, S.G., Rockwell, T.K., Briggs, R.W., Thakur, V.C., Jayangondaperumal, R., 2006. Paleoseismic evidence of great surface rupture earthquakes along the Indian Himalaya. J. Geophys. Res.-Solid Earth 111.
Kumar, S., Wesnousky, S.G., Jayangondaperumal, R., Nakata, T., Kumahara, Y., Singh, V., 2010. Paleoseismological evidence of surface faulting along the northeastern Himalayan front, India: timing, size, and spatial extent of great earthquakes. J. Geophys. Res.-Solid Earth 115.
Lave, J., Yule, D., Sapkota, S.N., Basant, K., Madden, C., Attal, M., Pandey, R., 2005. Evidence for a great medieval earthquake (∼1100 A.D.) in the Central Himalayas, Nepal. Science 307, 1302–1305.
Leonard, M., 2014. Self-consistent earthquake fault-scaling relations: update and extension to stable continental strike-slip faults. Bull. Seismol. Soc. Am. 104, 2953–2965.
Molnar, P., Chen, W.-P., Fitch, T.J., Tapponnier, P., Warsi, W.E.K., Wu, F.T., 1977. Structure and tectonics of the Himalaya: a brief summary of geophysical observations. Colloques Internationaux du D.N.R.S. Ecologie et Geologie de L'Himalaya 268, 269–294.
Molnar, P., Deng, Q.D., 1984. Faulting associated with large earthquakes and the average rate of deformation in central and eastern Asia. J. Geophys. Res. 89, 6203–6227.
NSC, 2015. National Seismological Center, Nepal. < http://www.seismonepal.gov.np/index.php?action=earthquakes&show=recent >).
Pant, M.R., 2002. A Step Towards a Historical Seismicity of Nepal. ADARSA. Pundit publications, Kathmandu, pp. 29–60.
Reimer, P.J., Bard, E., Bayliss, A., Beck, J.W., Blackwell, P.G., Ramsey, C.B., Buck, C.E., Cheng, H., Edwards, R.L., Friedrich, M., Grootes, P.M., Guilderson, T.P., Haflidason, H., Hajdas, I., Hatte, C., Heaton, T.J., Hoffmann, D.L., Hogg, A.G., Hughen, K.A., Kaiser, K.F., Kromer, B., Manning, S.W., Niu, M., Reimer, R.W., Richards, D.A., Scott, E.M., Southon, J.R., Staff, R.A., Turney, C.S.M., van der Plicht, J., 2013. INTCAL13 and marine13 radiocarbon age calibration curves 0–50,000 years Cal Bp. Radiocarbon 55, 1869–1887.
Seeber, L., Armbruster, J., 1981. Great detachment earthquakes along the Himalayan arc and long-term forecasting. In: Simpson, D.W., Richards, P.G. (Eds.), Earthquake Prediction: An International Review. AGU, Washington, D. C., pp. 215–242.
Stevens, V.L., Avouac, J.P., 2015. Interseismic coupling on the main Himalayan thrust. Geophys. Res. Lett. 42, 5828–5837.
Stevens, V.L., Avouac, J.P., 2016. Millenary M-w > 9.0 earthquakes required by geodetic strain in the Himalaya. Geophys. Res. Lett. 43, 1118–1123.
Upreti, B.N., Nakata, T., Kumahara, Y., Yagi, H., Okumura, K., Rockwell, T.K., Virdi, N.S., 2000. The latest active faulting in Southeast Nepal. In: Proceedings of the Hokudan International Symposium and School in Active Faulting, Awaji Island, Hyogo Japan, pp. 533–536.
Upreti, B.N., Kumahara, Y., Nakata, T., 2007. Paleoseismological study in the Nepal Himalaya—Present status. In: Proceedings of the Korea-Nepal Joint symposium on slope stability and landslides April 1, 2007, pp. 1–9.
Wesnousky, S.G., Kumahara, Y., Chamlagain, D., Pierce, I.K., Karki, A., Gautam, D., 2017a. Geological observations on large earthquakes along the Himalayan frontal fault near Kathmandu, Nepal. Earth Planet. Sci. Lett. 457, 366–375.
Wesnousky, S.G., Kumahara, Y., Chamlagain, D., Pierce, I.K., Reedy, T., Angster, S.J., Giri, B., 2017b. Large paleoearthquake timing and displacement near Damak in eastern Nepal on the Himalayan Frontal Thrust. Geophys. Res. Lett. 44, 8219–8226.
Wesnousky, S.G., Kumahara, Y., Nakata, T., Chamlagain, D., Neupane, P., 2018. New observations disagree with previous interpretations of surface rupture along the himalayan frontal thrust during the great 1934 Bihar-Nepal Earthquake. Geophys. Res. Lett. 45, 2652–2658.